S-I model of horizontal jet grouting reinforcement for soft soil

Ning Zhang[*1], Zhongyin Li[2], Qingsong Ma[2], Tianchi Ma[3,4], Xiaodong Niu[3,4],
Xixi Liu[3,4] and Tao Feng[3,4]

[1]*Institute of Hydroelectric and Geotechnical Engineering, North China Electric Power University, Beijing, 102206, China*
[2]*Beijing Sany Heavy Machinery Co., Ltd, Beijing 102226, China*
[3]*Shandong Provincial Key Laboratory of Ocean Engineering, Qingdao 266100, China*
[4]*Shandong Provincial Key Laboratory of Marine Environment and Geological Engineering, Ocean University of China,
266100 Qingdao, China*

Abstract.   A superposition-iteration (S-I) model is proposed to simulate the jet grouting pre-reinforcing impact for a shallow-buried tunnel. The common model is deduced by theoretical (force equilibrium) analysis and then transformed into the numerical formulation. After applying it to an actual engineering problem, the most obvious deficiency was found to be continuous error accumulation, even when the parameters change slightly. In order to address this problem, a superposition-iteration model is developed based on the basic assumption and superposition theory. First, the additional deflection between two successive excavation steps is determined. This is caused by the disappearance of the supporting force in the excavated zone and the soil pressure in the disturbed zone. Consequently, the final deflection can be obtained by repeatedly superposing the additional deflection to the initial deflection in the previous steps. The analytical solution is then determined with the boundary conditions. The superposition-iteration model is thus established. This model was then applied and found to be suitable for real-life engineering applications. During the calculation, the error induced by the ill-conditioned problem of the matrix is easily addressed. The precision of this model is greater compared to previous models. The sensitivity factors and their impact are determined through this superposition-iteration model.

Keywords: superposition-iteration; tunnel reinforcement; horizontal jet grouting; analytical solution

1. Introduction

The progress in reinforcement technology has led to improved tunnel construction in both hard rock and soft soils. (Chen *et al.* 2013, 2014). Horizontal jet grouting is one of the most effective methods in reinforcing tunnels, especially the shallow-buried type. The construction of a pipe shed reduces oil deformation by forming an arc concretion body during tunnel excavation. The umbrella arch method has been a viable alternative in tunnel excavation, and the umbrella arch pipe is very effective in minimizing surface settlement (Yasitli 2013). Owing to the excellent support provided by this structure, the soil pressure acting on the tunnel is released, thus improving the physical parameters and stability of the soil. Consequently, the tunnel face is stabilized, thus preventing tunnel collapse and settlement. Today, the length of the pipe shed is increasing with improvements in horizontal mechanical drilling technology, and even reaches 100 m in some engineering projects. This change undoubtedly enhances engineering quality and construction efficiency. However, it also increases the difficulty of stability calculations for the tunnel because each excavation step will cause the deflection accumulation of the pipe shed. Therefore, the

final settlement cannot be obtained unless the entire excavation process is simulated throughout the whole tunnel.

Various researchers have mathematically simulated the stability of tunnels. In previous analysis, the beam theory and arc shell theory have been widely used in pipe shed calculations. However, these two methods have proven to be limited in some aspects. In view of this, elastic foundation beam theory has been adopted as the common model for calculations. Wang *et al.* (2010) monitored ground subsidence and pore pressure changes around shallow tunnels through triaxial compression tests and numerical simulations. Yang *et al.* (2015) used the upper bound theorem of limit analysis, proposed two different curve function soil layers, and discussed the concrete shape of the subsidence surface using the proposed curve function. In recent years, special finite element method (FEM) software has been developed for underground reinforcement. This improvement makes the predefined structural elements embedded in commercial software available for simulating the reinforcement system, thus facilitating the entire simulation process. For example, Mazek (2014) considered the stress and strength parameters of sand with different densities by finite element analysis (FEA), and concluded that the different sand densities that have been neglected in surface displacement equation (SDE) have a significant impact on surface displacement during tunnel excavation Furthermore, Miranda *et al.* (2015) applied numerical simulation and inverse analysis

---

∗Corresponding author, Ph.D.
 E-mail: zning1125@ncepu.edu.cn

procedures to real-time observations of tunnel engineering data. Hong *et al.* (2014, 2015) performed a numerical parametric study on tension effects during tunneling and excavation by FEA.

The pipe end is generally simplified and regarded as the fixed end with vertical displacement in previous literature. Moreover, the loading effect on the influence zone behind the working face is not considered. Such simplification reduces the influence area compared to the actual situation, and therefore fails to reflect the real deformation. This analytical approach also depends on the experience of the designer. The processes involved consume considerable time and manual labor. Therefore, there is an urgent need for an effective model for horizontal jet grouting reinforcement calculation.

In this paper, the common model is first analyzed by transforming it into an analytical model, which is then analyzed by applying it to an actual engineering problem. The main deficiency observed is continuous error accumulation even with slight changes in parameters. In order to address this problem, a superposition-iteration (S-I) model is proposed based on the basic assumption and deformation superposition theory. In the formulation of force-equilibrium equations, the analytical solution is determined by analyzing each excavation step and the boundary conditions. Consequently, the S-I model is evaluated. It is shown that the accuracy of this model is better than that of the common model. This model is then applied to an actual engineering project in China and verified to be effective.

2. Deficiencies of the common model

2.1 Soil hypothesis and deformation law during tunnel excavation

The deformation law of soil ahead of the tunnel face is the foundation for the model establishment. This disturbed area is linear to the diameters of the tunnel. Model tests (Wu *et al.* (2016), Barla and Bzówka (2013), Han *et al.* (2012) and Li *et al.* (2017)) have shown that the disturbing area in the soil is 1D (tunnel diameter) ahead, and 2D above the shallow-buried tunnel face. Gioda and Locatelli (1999), Shen and Xu (2011) assumed that soil behavior is elastic. In order to propose the model, some basic assumptions are adopted.

The soils are considered as an isotropic continuum, in accordance with the Winkler assumption. The soil pressure is transmitted to be linear after the tunnel face has passed over. The prereinforced zone will still support the tunnel after it achieves stability. The disturbing zone moves forward along with the tunnel face, where the distance travelled is equal to the excavation length is identical to the excavation length. The deformation of the pre-reinforced zone can be superposed during the excavation procedure.

2.2 The beam effect for the jet grouting piles

The general monospar model can be established as shown in Fig. 1 and analyzed as:
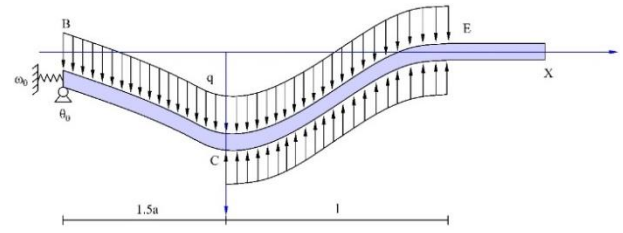

Fig. 1 The traditional common model of pre-reinforced zone

Fig. 1 demonstrates the common model for a shallow-buried tunnel. The pipe shed is simplified to be a monospar. Section BC is the excavated area without support. Section CE has not yet been excavated. These two areas are taken as the research object. The end of section BC is simplified and regarded as a hinge with vertical displacement. The excavating influence area of the tunnel is 1D. According to the theoretical analysis, the force equilibrium equations of this pipe shed can be written as

$$
\begin{cases}
\text{BC:} \dfrac{d^4 y_1}{dx^4} = \dfrac{bq}{EI} \\[2mm]
\text{CE:} \dfrac{d^4 y_2}{dx^4} + 4\lambda^4 y_2 = \dfrac{bq(D-x)}{EID} \\[2mm]
q = \dfrac{\varepsilon}{a_0 + b_0 \varepsilon}
\end{cases}
\tag{1}
$$

where y_1 and y_2 are the deflections of sections BC and CE in the pre-reinforced zone, respectively; q is the upper soil pressure of the pre-reinforced zone, a_0 and b_0 are the material parameters, EI is the bending rigidity of the pre-reinforced zone, b is the width of the pipe, and D is the diameter of the tunnel. $\lambda = \sqrt[4]{\dfrac{k}{4EI}}$, k is the stiffness coefficient of the elastic subgrade.

The general solution of the deflection equation can be obtained by integrating the differential equations in Eq. (1)

$$
\begin{aligned}
y_1 &= \frac{qbx^4}{24EI} + C_1 x^3 + C_2 x^2 + C_3 x + C_4 \\[2mm]
y_2 &= e^{\lambda x}(C_5 \cos \lambda x + C_6 \sin \lambda x) + \\[2mm]
&\quad e^{-\lambda x}(C_7 \cos \lambda x + C_8 \sin \lambda x) + \frac{q}{k} - \frac{qx}{KD}
\end{aligned}
\tag{2}
$$

where y_1 and y_2 are the deflections of sections BC and CE, respectively, and C_i ($i = 1, 2, 3,…$) are the coefficients during the integration of the Eq. (2).

We already know that the equations of the installation angle, bending moment, and shear force can be expressed as

$$
\begin{cases}
\theta = \dfrac{dy}{dx} \\[2mm]
M = -EI \dfrac{d\theta}{dx} = -EI \dfrac{d^2 y}{dx^2} \\[2mm]
Q = \dfrac{dM}{dx} = -EI \dfrac{d^3 y}{dx^3}
\end{cases}
\tag{3}
$$

Thus, the installation angle, bending moment, and shear force for sections BC and CE can be obtained by substituting Eq. (2) into Eq. (3)

where y_i is the deflection, θ is the installation angle, M is the bending moment, and Q is the shear force of sections BE and CE. The boundary and initial conditions of the general solution can be obtained based on the supporting conditions

$$\begin{cases} y_B = y_1 \big|_{x=-1.5a} = \omega_0 \\ \theta_B = y_1' \big|_{x=-1.5a} = \theta_0 \end{cases}$$

$$\begin{cases} y_C = y_1 \big|_{x=0} = y_2 \big|_{x=0} \\ \theta_C = y_1' \big|_{x=0} = y_2' \big|_{x=0} \\ M_C = EIy_1'' \big|_{x=0} = EIy_2'' \big|_{x=0} \\ Q_C = EIy_1''' \big|_{x=0} = EIy_2''' \big|_{x=0} \end{cases} \qquad (6)$$

$$\begin{cases} M_E = EIy_2'' \big|_{x=l} = 0 \\ Q_E = EIy_2''' \big|_{x=l} = 0 \end{cases}$$

where y_B, y_C, y_E are the displacements at points B, C, and E, respectively. The displacement at point C is identical to that between sections BC and CE. The displacement at point B and bending moment at end point E are the initial conditions.

The boundary condition Eq. (6) is substituted to deflection Eqs. (4)-(5); thus, the equations for coefficient can be obtained as follows

$$\begin{cases} 27a^3 C_1 - 18a^2 C_2 + 12aC_3 - 8C_4 = \dfrac{27qba^4}{16EI} - 8\omega_0 \\ 27a^2 C_1 - 12a^2 C_2 + 4C_3 = \dfrac{27qba^3}{12EI} - 4\theta_0 \\ C_4 - C_5 - C_7 = \dfrac{q}{k} \\ C_3 - \lambda C_5 - \lambda C_6 + \lambda C_7 - \lambda C_8 = -\dfrac{q}{kD} \\ C_2 - 2\lambda^2 C_6 + 2\lambda^2 C_8 = 0 \\ 3C_1 + \lambda^3 C_5 - \lambda^3 C_6 - \lambda^3 C_7 - \lambda^3 C_8 = 0 \\ e^{\lambda x}(-C_5 \sin \lambda x + C_6 \cos \lambda x) \\ \quad + e^{-\lambda x}(C_7 \sin \lambda x - C_8 \cos \lambda x) = 0 \\ e^{\lambda x}\left[-C_5(\sin \lambda x + \cos \lambda x) + C_6(\cos \lambda x - \sin \lambda x)\right] \\ \quad + e^{-\lambda x}\left[C_7(\cos \lambda x - \sin \lambda x) + C_8(\sin \lambda x + \cos \lambda x)\right] = 0 \end{cases} \qquad (7)$$

Because Eq. (7) is much more complex, it can be transformed into the matrix

$$\begin{bmatrix} 27a^3 & -18a^2 & 12a & -8 & 0 & 0 & 0 & 0 \\ 27a^2 & -12a & 4 & 0 & 0 & 0 & 0 & 0 \\ 0 & 0 & 0 & 1 & -1 & 0 & -1 & 0 \\ 0 & 0 & 1 & 0 & -\lambda & -\lambda & \lambda & -\lambda \\ 0 & 1 & 0 & 0 & 0 & -2\lambda^2 & 0 & 2\lambda^2 \\ 3 & 0 & 0 & 0 & \lambda^3 & -\lambda^3 & -\lambda^3 & -\lambda^3 \\ 0 & 0 & 0 & 0 & \varphi_1 & \varphi_2 & \varphi_3 & \varphi_4 \\ 0 & 0 & 0 & 0 & \varphi_5 & \varphi_6 & \varphi_7 & \varphi_8 \end{bmatrix} \begin{bmatrix} C_1 \\ C_2 \\ C_3 \\ C_4 \\ C_5 \\ C_6 \\ C_7 \\ C_8 \end{bmatrix} = \begin{bmatrix} \dfrac{27qba^4}{16EI} - 8y_0 \\ \dfrac{27qba^3}{12EI} - 4\theta_0 \\ \dfrac{q}{k} \\ -\dfrac{q}{kD} \\ 0 \\ 0 \\ 0 \\ 0 \end{bmatrix} \qquad (8)$$

where

$$\begin{cases} \varphi_1 = -e^{\lambda l} \cdot \sin \lambda l \\ \varphi_2 = e^{\lambda l} \cdot \cos \lambda l \\ \varphi_3 = e^{-\lambda l} \cdot \sin \lambda l \\ \varphi_4 = -e^{\lambda l} \cdot \cos \lambda l \\ \varphi_5 = -e^{\lambda l} \cdot (\sin \lambda l + \cos \lambda l) \\ \varphi_6 = e^{\lambda l} \cdot (\cos \lambda l - \sin \lambda l) \\ \varphi_7 = e^{-\lambda l} \cdot (\cos \lambda l - \sin \lambda l) \\ \varphi_8 = e^{-\lambda l} \cdot (\sin \lambda l + \cos \lambda l) \end{cases}$$
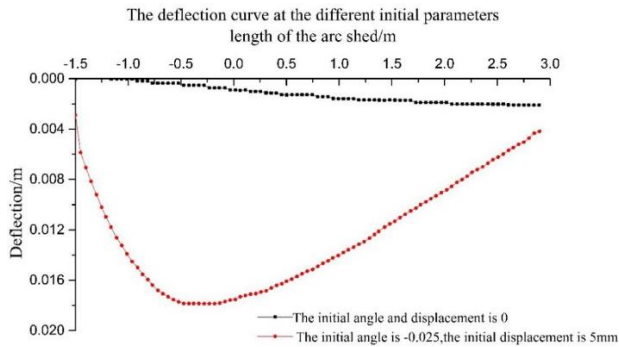

Fig. 2 The application of the actual pipe shed in Liuyanghe Tunnel, China

$$\begin{cases} \theta_1 = y_1' = \dfrac{qbx^3}{6EI} + 3C_1 x^2 + 2C_2 x + C_3 \\ M_1 = -EI\dfrac{d\theta_1}{dx} = -EI\left(\dfrac{qbx^2}{2EI} + 6C_1 x + 2C_2\right) \\ Q_1 = \dfrac{dM_1}{dx} = -EI\dfrac{d^3 y}{dx^3} = -EI\left(\dfrac{qbx}{EI} + 6C_1\right) \end{cases} \qquad (4)$$

$$\begin{cases} \theta_2 = \lambda e^{\lambda x}\left[C_5(\cos \lambda x - \sin \lambda x) + C_6(\sin \lambda x + \cos \lambda x)\right] \\ \qquad - \lambda e^{-\lambda x}\begin{bmatrix} C_7(\sin \lambda x + \cos \lambda x) \\ -C_8(\cos \lambda x - \sin \lambda x) \end{bmatrix} - \dfrac{q}{KD} \\ M_2 = -EI\dfrac{d\theta_2}{dx} \\ \quad = -2EI\lambda^2 \begin{bmatrix} e^{\lambda x}(C_6 \cos \lambda x - C_5 \sin \lambda x) \\ + e^{-\lambda x}(C_7 \sin \lambda x - C_8 \cos \lambda x) \end{bmatrix} \\ Q_2 = \dfrac{dM_2}{dx} = -EI\dfrac{d^3 y}{dx^3} \\ \quad = -2EI\lambda^3 \begin{Bmatrix} e^{\lambda x}\begin{bmatrix} C_6(\cos \lambda x - \sin \lambda x) \\ -C_5(\sin \lambda x + \cos \lambda x) \end{bmatrix} \\ + e^{-\lambda x}\begin{bmatrix} C_7(\cos \lambda x - \sin \lambda x) \\ + C_8(\sin \lambda x + \cos \lambda x) \end{bmatrix} \end{Bmatrix} \end{cases} \qquad (5)$$

The deflection curve at the different initial parameters

Fig. 3 The calculation results of the common model in actual engineering

2.3 Effect of the common model

Prototype engineering in Liuyanghe, China, is used as an example to test this common model. During the analysis, the soil pressure was calculated as a whole soil column. The region of this soil column was determined from the excavation zone to the disturbing zone. This simplification was made to ensure that the burial depth was shallow enough (H < 2D, where H is the depth of the overlying soil and D is the diameter of the tunnel). Thus, the soil pressure can be obtained as

$$q = 50\% \times gh = 81 KPa$$

The range of the disturbing area in the soil is calculated according to the Mohr–Coulomb theory

$$l = H \tan(\frac{\pi}{4} - \frac{\varphi}{2}) = 4.616m$$

where φ is the inner cohesion angle.

The disturbing zone is determined to be 5 m for safety purposes. The loading zone of the monosopar includes the nonsupporting area behind the tunnel face. The disturbing zone endures the soil disturbing loading. The range is 5 m away from the excavating zone to the tunnel face. The coefficient of subgrade reaction is 3.5 × 104 kN/m3. The diameter of the jet grouting is 0.8 m, the elasticity modulus of the jet grouting pile is 2 GPa, the initial settlement is ω_0=3 mm, and the installation angle is θ_0=-1.5. The excavation process is shown in Fig. 2.

If the parameters are substituted into Eq. (8), the coefficient C_i (i = 1, 2, 3, … , 8) can then be determined and the model is finally obtained. Thus, the deflection curve along the whole tunnel can be drawn given the parameters. An example at different parameters is compared and demonstrated in Fig. 2. The initial angles and initial deflections are 0, 0 and -0.025, 5 mm, respectively.

Fig. 3 shows that the deflection greatly varies with changing parameters. However, initial parameters such as the initial settlement ω_0 and installation angle θ_0 are difficult to determine. The deflection can vary widely even when parameters change only slightly. This phenomenon shows that the assumptions of the common model are not rational, and is analyzed below.

During the model development, the connection between the beam and support is simplified and regarded as a fixed end with vertical displacement. Additionally, the excavation disturbance of the forward soil is not considered. The loading effect behind the tunnel face and the entity effect of the monospar are also ignored. Only the deformation of the non-supporting area is calculated. These assumptions reduce the influence area of the pre-reinforced zone. Consequently, the common model is shown to be irrational in simulating tunnel excavation. Therefore, a new model is urgently needed that represents actual shallow-buried tunnels.

3. Establishment of the Superposition-Iteration model

In previous literature, some deformation-superposition based methods have been utilized. However, this superposition just involves external forces along with the supporting force of the pre-reinforced structures, as well as the durable effect of the soil pressure after tunnel excavation. This simplification suggests that the unit deflection is directly proportional to the excavation steps. The deflection calculated by this method will therefore be infinity, with the excavation steps continuously increasing. This obviously does not reflect actual engineering applications. In order to address these deficiencies, an S-I model was developed for the pre-reinforced shallow-buried tunnel.

3.1 Basic assumption and soil pressure determination

In order to develop the model, some assumptions were made to reduce the complexity. First, the soil of the tunnel is regarded as being linear isotropic elastic and is assumed to conform to the Winkler assumption. Therefore, the deformation of the soil above the tunnel cannot resume during the excavation process, i.e., there is no rebound. For security, the soil pressure behind the tunnel face is calculated as the overall soil column. The value is determined to be zero from the tunnel face to the boundary of the influence area.

The boundary conditions of the monospar can be divided into the supporting zone, excavating zone, disturbing zone, and non-disturbing zone. Among them, the stiffness of the supporting zone is reduced in consideration of the carry effect. The area of the excavating zone is the length of a single footage; thus, it can be regarded as the non-supporting zone.

The disturbing zone is the stress relaxation area caused by the working face excavation. The surrounding rock pressure is determined to be the monolithic column pressure from the tunnel face to the disturbing boundary.

Notes: 1. the excavated zone with supporting; 2. the excavated zone without supporting; 3. the unexcavated zone; 4. the initial supporting; 5. the concrete umbrella arc; 6. steel arc centering; 7. tunnel face; 8. surrounding rocks; 9. fractured face

There are three kinds of coefficient of subgrade reactions in the built model. The basic soil coefficient of subgrade reaction was obtained from actual measurements.
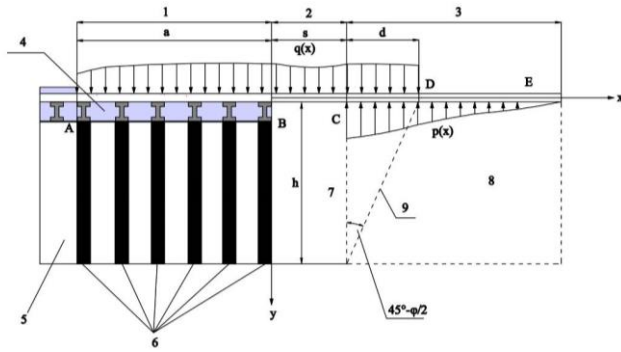
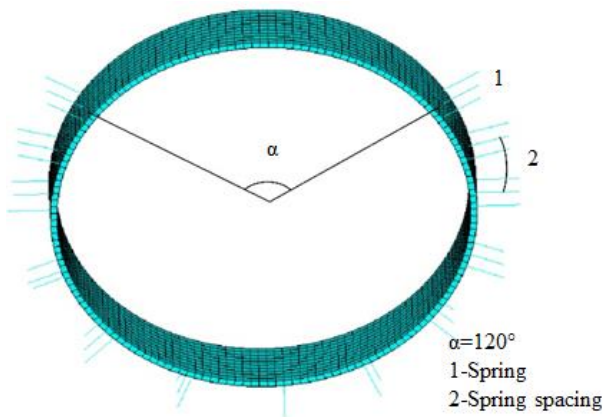Fig. 4 The zone distribution and soil pressure for the monospar

Fig. 5 The finite element model for the coefficient of subgrade reactions calculation
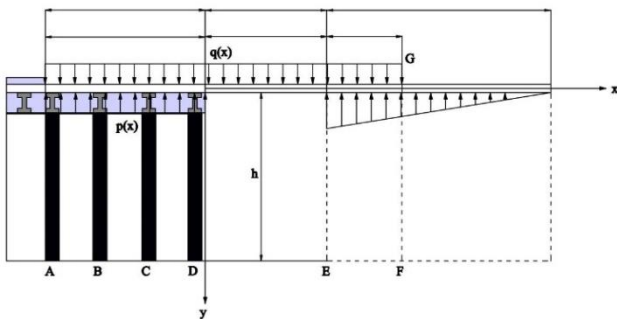

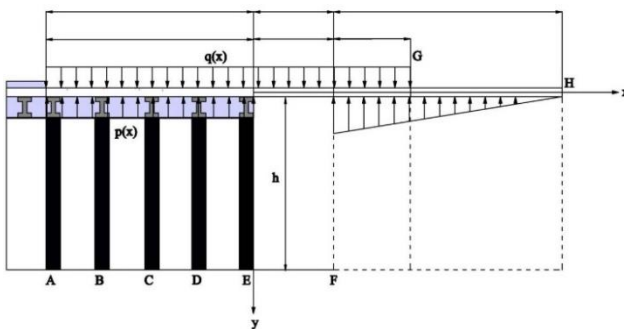Fig. 6 The analytical model of the *n*th excavation step

Fig. 7 The analytical model of the (*n+1*)th excavation step

The coefficient of subgrade reaction in the excavation zone was determined to be zero. The coefficient of subgrade reaction in the supporting zone was determined from the
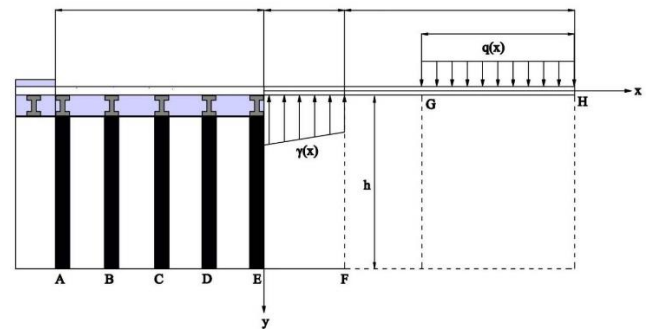

Fig. 8 The analytical model for the additional loading

results of FE calculations (Fig. 5). A model was established according to the characteristics of the lining structure. Under the impact of loosening soil pressure, the lining range of 90o-120o deformed inside the tunnel, leading to the detachment zone. Therefore, there was no spring arranged, and the layer deformed toward the arc and side wall. Consequently, the elastic resistance zone emerged. The springs were thus utilized to replace the restraint effect of the rock mass. Its elastic coefficient was determined by the actual stiffness coefficient; the springs were also arranged at the invert.

This model can be demonstrated through the iteration between the nth excavation step (*n* can arbitrarily be 0, 1, 2, 3, …) and the (*n+1*)th step. Figs. 6 and 7 show the loading and situation of the nth and (*n+1*)th excavation steps, respectively.

As seen in Fig. 6, section AD is the supporting area, while section DE is the excavated area without supporting. q(x) is the soil pressure in sections AB, BC, CD, and EG of the pre-reinforced zone; p(x) is the subgrade reaction of sections AB, BC, and CD; and g(x) is the subgrade reaction in section EF.

As Fig. 7 shows, a new excavation step is conducted (i.e., section EF is excavated) based on the working condition in Fig. 6. Then, section EF is the excavated area without supporting, while the whole section AE (AB, BC, CD, and DE) is the excavated area with supporting. We have already assumed that the relaxation region moved forward at the same distance as the excavation step, section GH transformed into the disturbing zone along with the excavation of section EF. Therefore, there are two changes when comparing Figs.7 and 6. One is that section EF was excavated without supporting. The other is that section GH turns into the relaxation area. During loading, the subgrade reaction γ(x) in section EF disappeared as it was excavated. Second, extra soil pressure appeared in section GH, which is q(x). These changes are demonstrated in Fig. 6. q(x) is the soil pressure of the pre-reinforced zone, i.e., section AG and p′(x) are the subgrade reactions of the entire section AE.

Consequently, the loading in Fig. 7 can be expressed by the loading in Fig. 6 superposed to these two changes. As the deflection can be superposed, the deflection in Fig.6 can be calculated by the deflection in Fig. 7 superposed to the additional deflection in Fig. 8. This additional deflection can be calculated by the loading change from Fig.6 to Fig. 7, which is shown in Fig. 8.

Fig. 8 shows the analytical model for the additional loading. Therefore, the final loading can be calculated by superposing -γ(x) in section EF and q(x) in section GH to the working condition in Fig. 6. Consequently, the final deformation in Fig. 7 is the settlement of the working condition in Fig.6 superposed to the deflection induced by the excavation in Fig. 8. This superposition deformation was caused by -γ(x) and q′(x) in sections EF and GH, respectively.

3.2 Establishment of the model

During the excavation of the pre-reinforced tunnel, the deflection curve of the (*n+1*)th excavation step is the deflection curve of the nth step superposed to the addition deflection of the (*n+1*)th step.

The model in Fig. 8 represents the additional loading in the arbitrary excavation step. The additional deflection of this step can be calculated by the elastic subgrade. The pre-reinforced zone can be divided into sections AB, BC, CD, DE, and EF based on the boundary conditions. The coordinate is established according to Fig. 8. Thus, the additional deflection differential equation (i.e., the force equilibrium equation) can be expressed as

$$
\begin{cases}
AD: \dfrac{d^4 y_1}{dx^4} + 4\lambda^4 y_1 = 0 \\[2mm]
DE: \dfrac{d^4 y_2}{dx^4} = -\dfrac{b\gamma(x)}{EI} \\[2mm]
FG: \dfrac{d^4 y_3}{dx^4} + 4\lambda^4 y_3 = 0 \\[2mm]
GH: \dfrac{d^4 y_4}{dx^4} + 4\lambda^4 y_4 = \dfrac{bq}{EI} \\[2mm]
HI: \dfrac{d^4 y_5}{dx^4} + 4\lambda^4 y_5 = 0
\end{cases}
\tag{9}
$$

where γ(x) is the known function of the nth step. The general formulation can be expressed as

$$
\begin{aligned}
\gamma(x) &= e^{\lambda x}(A_1 \cos \lambda x + A_2 \sin \lambda x)\cdot K \\
&\quad + e^{-\lambda x}(A_3 \cos \lambda x + A_4 \sin \lambda x)\cdot K + A_5 \cdot K
\end{aligned}
\tag{10}
$$

where A_i ($i = 1, 2, 3, 4, 5$) are the known parameters. In $\lambda = \sqrt[4]{\dfrac{k}{4EI}}$, k is the rigidity of the elasticity foundation. The deflection of the beam is assumed to be y_i, the installation angle is θ_i, the bending moment is M_i, and the shearing force is Q_i. Based on this analysis, Eq. (10) is substituted into Eq. (9), and the general formulation of the deflection can be obtained.

$$
\begin{cases}
y_1 = e^{\lambda x}(C_1 \cos \lambda x + C_2 \sin \lambda x) \\
\qquad + e^{-\lambda x}(C_3 \cos \lambda x + C_4 \sin \lambda x) \\
y_2 = e^{\lambda x}(A_1 \cos \lambda x + A_2 \sin \lambda x) \\
\qquad + e^{-\lambda x}(A_3 \cos \lambda x + A_4 \sin \lambda x)\cdot k \\
\qquad + \dfrac{A_5 \cdot k x^4}{24} + C_5 x^3 + C_6 x^2 + C_7 x + C_8 \\
y_3 = e^{\lambda x}(C_9 \cos \lambda x + C_{10} \sin \lambda x) \\
\qquad + e^{-\lambda x}(C_{11} \cos \lambda x + C_{12} \sin \lambda x) \\
y_4 = e^{\lambda x}(C_{13} \cos \lambda x + C_{14} \sin \lambda x) \\
\qquad + e^{-\lambda x}(C_{15} \cos \lambda x + C_{16} \sin \lambda x) + \dfrac{q}{k} \\
y_5 = e^{\lambda x}(C_{17} \cos \lambda x + C_{18} \sin \lambda x) \\
\qquad + e^{-\lambda x}(C_{19} \cos \lambda x + C_{20} \sin \lambda x)
\end{cases}
\tag{11}
$$

The boundary equations of the deflection equation can be obtained according to the supporting condition

$$
A: \begin{cases} M_1 = EI y_1'' = 0 \\ Q_1 = EI y_1''' = 0 \end{cases}
$$

$$
B: \begin{cases} y_1 = y_2 \\ \theta_2 = y_1' = y_2' \\ M_2 = EI y_1'' = EI y_2'' \\ Q_2 = EI y_1''' = EI y_2''' \end{cases}
$$

$$
C: \begin{cases} y_2 = y_3 \\ \theta_3 = y_2' = y_3' \\ M_3 = EI y_2'' = EI y_3'' \\ Q_3 = EI y_2''' = EI y_3''' \end{cases}
\tag{12}
$$

$$
D: \begin{cases} y_3 = y_4 \\ \theta_4 = y_3' = y_4' \\ M_4 = EI y_3'' = EI y_4'' \\ Q_4 = EI y_3''' = EI y_4''' \end{cases}
$$

$$
F: \begin{cases} M_6 = EI y_5'' = 0 \\ Q_6 = EI y_5''' = 0 \end{cases}
$$

Eq. (11) is substituted into Eq. (12); thus, the coefficient equations can be established. However, these will be much more complex equations. The solution is the additional deflection equation for each excavation step of the monospar. Given the complexity of this equation, it can be written as a large matrix, which can be calculated by the MATLAB software. These processes and steps are repeated, and the general formulation of the solution for each beam section can be obtained as follows

$$
\begin{aligned}
y &= e^{\lambda x}(C_1 \cos \lambda x + C_2 \sin \lambda x) \\
&\quad + e^{-\lambda x}(C_3 \cos \lambda x + C_4 \sin \lambda x) \\
&\quad + C_5 x^4 + C_6 x^3 + C_7 x^2 + C_8 x + C_9
\end{aligned}
\tag{13}
$$

Eq. (13) is the general formulation of the solution.

4. Comparison and verification

In order to validate the utility of this superposition model, it was applied to monospar engineering. The results were calculated based on real-time monitoring data (Yanglong *et al.* 2015). The utility of this superposition model was also compared to the previous common model. In actual engineering applications, the tunnel was a straight wall arc with a diameter of 4 m and burial depth of 14 m. The initial supports were steel arcs and steel fabric reinforcement with jet cement. The tunnel was supported by a long pipe shed with an outer diameter of 600 mm, width of 12 mm, and length of 36 m. During the excavation process, the minor step method was adopted with a length of 1.5 m and footage of 5 m. The daily footage of the tunnel was determined to be 2 m. Therefore, the footage of the excavation zone was 2 m. The parameters of the soil are listed in Table 1.

According to the Mohr-Coulomb theory, the influence area of this tunnel face is 3 m and the loading of the monospar is 67.4 kN/m. Based on these parameters, the calculated rigidity of the elasticity subgrade beam was 71840 kPa/m. The end of the beam was set as the fixed end

Table 1 The parameters of the applied tunnel for the superposed model

Unit volume/kN/m	20.3
Modulus of compression/MPa	31.8
Poisson ratio	0.28
Cohesion/kPa	35.2
Internal friction angle	33
Stiffness coefficient/(kPa/m)	5.5e4
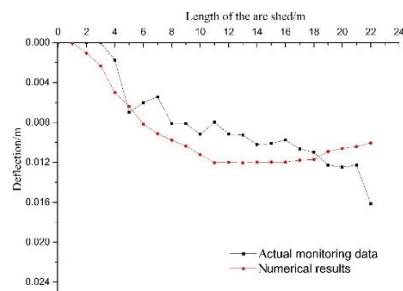
Fig. 9 The result of the calculation by adopting the S-I model

Fig. 10 The sensitivity factors impact law by the S-I model

in the first excavation step. The parameters and excavation steps were substituted into the MATLAB software to obtain the results.

The initial value of each calculation step corresponded to the result of the previous step. Therefore, the errors in each step can accumulate in the latter calculation steps. This phenomenon reflects the actual monitoring result because monospar deformation at each excavation step is related to the rotation angle and displacement of the previous excavation. Moreover, the installation angle and displacement at each step can influence the subsequent steps. This shows that the beam effect of the jet grouting pipe shed can be simulated by the S-I model. The deflection of the whole tunnel is shown in Fig. 9.

As the Fig. 9 demonstrates, the result of the model conforms to the actual monitoring data. Therefore, the precision of the whole calculation process is sufficiently high. This demonstrates that the S-I model can be used for actual engineering calculations. During the calculation procedure, the conditional number of the matrix was well addressed. The value is negligible at 0.00015 m when the superposition displacement was 4 m away from the end of the monospar. Therefore, the disturbing area was determined to be 8 m forward and behind the tunnel face.

5. Application in sensitivity factors analysis

The sensitivity factors during the arc shed supporting are needed for a more in-depth study. Understanding the effect of sensitive factors can explain the impact mechanism, and thus optimize the design of the arc shed.

Fig. 10 shows that the peak deflection decreases with increasing thickness of the arc shed, when it is less than 0.8 m. It remains stable when it becomes greater than 0.8 m. The thickness of the arc shed is no longer the main factor in
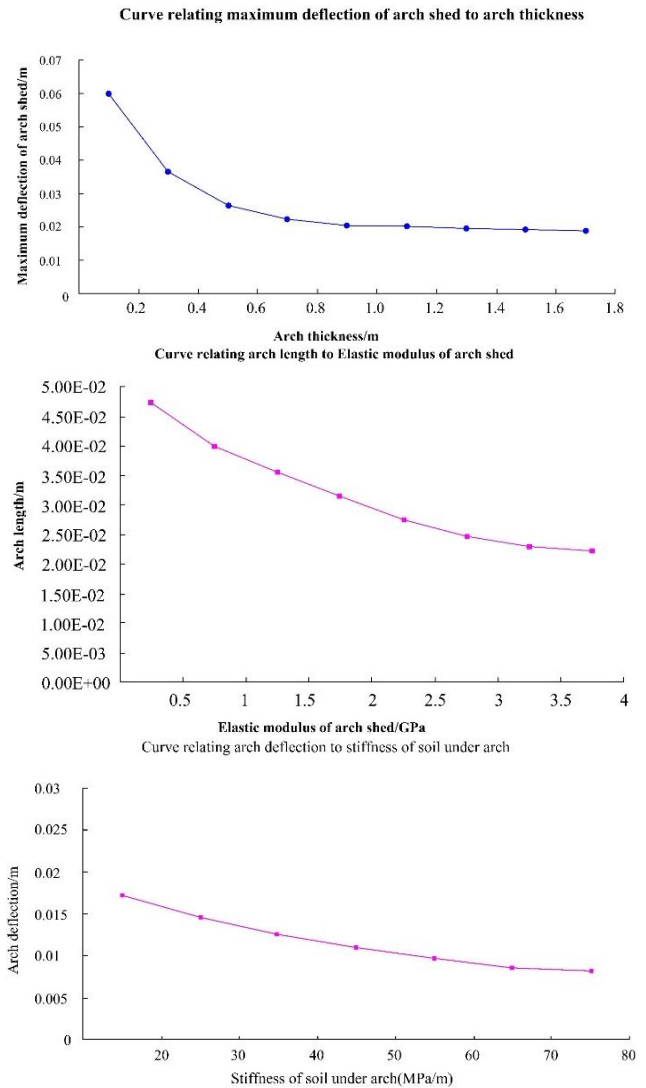
the settlement of the arc. The whole subsides occurs throughout the entire tunnel. Therefore, increasing the thickness of the arc shed, i.e., the diameter of the jet grouting, will not be effective.

The peak deflection slowly decreased with increasing elastic modulus of the arc shed. This basically represents the linear change. The peak deflection approaches a constant when the elastic modulus reaches 4 GPa. Then, the stiffness of the arc shed will no longer work. The whole subsides occurs throughout the entire tunnel. Therefore, it will not work by increasing the stiffness of the arc shed. The optimum effect occurs only when the stiffness of the arc shed and soil match each other.

The stiffness of the arc shed greatly influenced the peak deflection of the tunnel. However, the impact decreased when the stiffness reached a certain value. For example, when the diameter of the jet grouting pile reached 0.8 m, or the elastic modulus reached 4 GPa. The stiffness of the soil becomes the main factor that determines the deflection of the arc shed. The peak deflection decreases with increasing stiffness of the soil under the arc shed. It mostly presents a linear relationship. The peak deflection tends to be 5 mm with increasing stiffness of the soil.

6. Conclusions

The common model for a pre-reinforced shallow-buried tunnel was introduced and evaluated by theoretical analysis. It was applied in actual engineering and found to be deficient because of error accumulation. In order to address this deficiency and improve the precision of the model for pre-reinforcement, an S-I model was proposed based on the superposition theory. The additional deflection can be superposed to the former deflection curve to obtain the deflection in the latter step. This was induced by the disappearance of the supporting force in the excavated zone, and the appearance of soil pressure in the disturbed zone. Consequently, the S-I model was evaluated. By applying it to actual engineering, it was found to be in agreement with real-time results. The error induced by the ill-conditioned problem of the matrix was easily addressed during the calculation process. In addition, the results show that the precision of the whole calculation process improved. The sensitive factors and their impact were determined with this S-I model.

Acknowledgements

References

Barla, M. and Bzowka, J. (2013), "Comparing numerical alternatives to model jet grouting in tunnels", *Elec. J. Geotech. Eng.*, **18**, 2997-3008.

Chen, G.Q, Li, T.B., Zhang, G.F., Yin, H.Y. and Zhang, H. (2014). "Temperature effect of rock burst for hard rock in deep-buried tunnel", *Nat. Hazards*, **72**(2), 915-926.

Chen, G.Q., Li, T.B., Gao, M.B., Chen, Z.Q. and Xiang, T.B. (2013), "Deformation warning and dynamic control of dangerous disaster for large underground caverns", *Disaster Adv.*, **6**(s1), 422-430.

Gioda, G. and Locatelli, L. (1999), "Back analysis of the measurements performed during the excavation of a shallow tunnel in sand", *J. Numer. Anal. Meth. Geomech.*, **23**(13), 1407-1425.

Han, W., Liu, S., Zhang, D., and Du, G. (2012), "Field behavior of jet grouting pile under vacuum preloading of soft soils with deep sand layer", *Proceedings of the GeoCongress 2012: State of the Art and Practice in Geotechnical Engineering*, Oakland, California, U.S.A., March

Ho, C.E. (2011), "Evaluation of jet grout formation in soft clay for tunnel excavation", *Proceedings of the Geo-Frontiers 2011: Advances in Geotechnical Engineering*, Dallas, Texas, U.S.A., March.

Hong, Y., Ng, C.W.W. and Wang, L.Z. (2014), "Initiation and failure mechanism of base instability of excavations in clay triggered by hydraulic uplift", *Can. Geotech. J.*, **52**(5), 599-608

Hong, Y., Soomro, M.A., Ng, C.W.W., Wang, L.Z., Yan, J.J. and Li, B. (2015), "Tunnelling under pile groups and rafts: Numerical parametric study on tension effects", *Comput. Geotech.*, **68**, 54-65.

Li, Y.L, Sun, Y.T., Li, B. and Xu, Z.G. (2017), "Penalty function-based method for obtaining a reliability indicator of gravity dam stability", *Comput. Geotech.*, **81**, 19-25.

Mazek, S.A. (2014), "Evaluation of surface displacement equation due to tunnelling in cohesionless soil", *Geomech. Eng.*, **7**(1), 55-73.

Miranda, T., Dias, D., Pinheiro, M. and Eclaircy-Caudron, S. (2015), "Methodology for real-time adaptation of tunnels support using the observational method", *Geomech. Eng.*, **8**(2), 153-171.

Oke, J., Vlachopoulos, N. and Marinos, V. (2014), "Umbrella arch nomenclature and selection methodology for temporary support systems for the design and construction of tunnels", *Geotech. Geol. Eng.*, **32**(1), 97-130.

Shen, S.L. and Xu, Y.S. (2011), "Numerical evaluation of land subsidence induced by groundwater pumping in Shanghai", *Can. Geotech. J.*, **48**(9), 1378-1392.

Wang, Z., Wong, R.C.K. and Heinz, H. (2010), "Assessment of long-term behaviour of a shallow tunnel in clay till", *Geomech. Eng.*, **2**(2), 107-123.

Wu, Y.D., Diao, H.G., Ng, C.W., Liu, J. and Zeng, C.C. (2016), "Investigation of ground heave due to jet grouting in soft clay", *J. Perform. Constr. Fac.*, **30**(6), 06016003.

Yang, X.L. and Yan, R.M. (2015), "Collapse mechanism for deep tunnel subjected to seepage force in layered soils", *Geomech. Eng.*, **8**(5), 741-756.

Yanlong, L., Shouyi, L., Yang, Y. and Xing, T. (2015), "Temperature stress and surface insulation measures of concrete face slabs during cold wave period", *J. Civ. Eng.*, **13**(4), 501-507.

Yasitli, N.E. (2013), "Numerical modeling of surface settlements at the transition zone excavated by New Austrian Tunneling Method and Umbrella Arch Method in weak rock", *Arab. J. Geosci.*, **6**(7), 2699-2708.

Yuan, Y.C., Li, S.C., Zhang, Q.Y., Li, L.P., Shi, S.S. and Zhou, Z.Q. (2016), "Risk assessment of water inrush in karst tunnels based on a modified grey evaluation model: Sample as Shangjiawan Tunnel", *Geomech. Eng.*, **11**(4), 493-513.

CC

Appendix: The deduction and solution of the model

A.1 The initial excavation step

According to the established model, the initial excavation step can be calculated. Section AB is assumed to be l and the differential equations of the deflection are

$$
\begin{cases}
OA: \dfrac{d^4 y_1}{dx^4} = \dfrac{bq}{EI} \\
AB: \dfrac{d^4 y_2}{dx^4} + 4\lambda^4 y_2 = \dfrac{bq}{EI} \\
BC: \dfrac{d^4 y_3}{dx^4} + 4\lambda^4 y_3 = 0
\end{cases}
\tag{14}
$$

The general solution can be

$$
\begin{cases}
y_1 = \dfrac{qbx^4}{24EI} + C_1 x^3 + C_2 x^2 + C_3 x + C_4 \\
y_2 = e^{\lambda x}(C_5 \cos \lambda x + C_6 \sin \lambda x) \\
\quad + e^{-\lambda x}(C_7 \cos \lambda x + C_8 \sin \lambda x) + \dfrac{q}{k} \\
y_3 = e^{\lambda x}(C_9 \cos \lambda x + C_{10} \sin \lambda x) \\
\quad + e^{-\lambda x}(C_{11} \cos \lambda x + C_{12} \sin \lambda x)
\end{cases}
\tag{15}
$$

The boundary conditions of the different beam ends are obtained as

$$
\begin{aligned}
&O: \begin{cases} M_1 = EIy_1'' = 0 \\ Q_1 = EIy_1''' = 0 \end{cases} \\[4pt]
&A: \begin{cases} y_1 = y_2 \\ \theta_2 = y_1' = y_2' \\ M_2 = EIy_1'' = EIy_2'' \\ Q_2 = EIy_1''' = EIy_2''' \end{cases} \\[4pt]
&B: \begin{cases} y_2 = y_3 \\ \theta_3 = y_2' = y_3' \\ M_3 = EIy_2'' = EIy_3'' \\ Q_3 = EIy_2''' = EIy_3''' \end{cases} \\[4pt]
&C: \begin{cases} M_4 = EIy_3'' = 0 \\ Q_4 = EIy_3''' = 0 \end{cases}
\end{aligned}
\tag{16}
$$

A.2 The second excavation step

The deflection equation in the second excavation step is Eq. (17)

$$
\begin{cases}
y_1 = e^{\lambda x}(C_1 \cos \lambda x + C_2 \sin \lambda x) + e^{-\lambda x}(C_3 \cos \lambda x + C_4 \sin \lambda x) \\
y_2 = e^{\lambda x}(A_1 \cos \lambda x + A_2 \sin \lambda x) + e^{-\lambda x}(A_3 \cos \lambda x + A_4 \sin \lambda x)\cdot k + \frac{A_5 \cdot kx^4}{24} + C_5 x^3 + C_6 x^2 + C_7 x + C_8 \\
y_3 = e^{\lambda x}(C_9 \cos \lambda x + C_{10} \sin \lambda x) + e^{-\lambda x}(C_{11} \cos \lambda x + C_{12} \sin \lambda x) \\
y_4 = e^{\lambda x}(C_{13} \cos \lambda x + C_{14} \sin \lambda x) + e^{-\lambda x}(C_{15} \cos \lambda x + C_{16} \sin \lambda x) + \frac{q}{k} \\
y_5 = e^{\lambda x}(C_{17} \cos \lambda x + C_{18} \sin \lambda x) + e^{-\lambda x}(C_{19} \cos \lambda x + C_{20} \sin \lambda x) \\[4pt]
y_1' = \lambda e^{\lambda x}\left[C_1(\cos \lambda x - \sin \lambda x) + C_2(\sin \lambda x + \cos \lambda x)\right] - \lambda e^{-\lambda x}\left[C_3(\sin \lambda x + \cos \lambda x) + C_4(\sin \lambda x - \cos \lambda x)\right] \\
y_2' = k\lambda e^{\lambda x}\left[A_1(\cos \lambda x - \sin \lambda x) + A_2(\sin \lambda x + \cos \lambda x)\right] - \lambda e^{-\lambda x}\left[A_3(\sin \lambda x + \cos \lambda x) + A_4(\sin \lambda x - \cos \lambda x)\right] \\
\quad + \frac{A_5 \cdot kx^3}{6} + 3C_5 x^2 + 2C_6 x + C_7 \\
y_3' = \lambda e^{\lambda x}\left[C_9(\cos \lambda x - \sin \lambda x) + C_{10}(\sin \lambda x + \cos \lambda x)\right] - \lambda e^{-\lambda x}\left[C_{11}(\sin \lambda x + \cos \lambda x) + C_{12}(\sin \lambda x - \cos \lambda x)\right] \\
y_4' = \lambda e^{\lambda x}\left[C_{13}(\cos \lambda x - \sin \lambda x) + C_{14}(\sin \lambda x + \cos \lambda x)\right] - \lambda e^{-\lambda x}\left[C_{15}(\sin \lambda x + \cos \lambda x) + C_{16}(\sin \lambda x - \cos \lambda x)\right] \\
y_5' = \lambda e^{\lambda x}\left[C_{17}(\cos \lambda x - \sin \lambda x) + C_{18}(\sin \lambda x + \cos \lambda x)\right] - \lambda e^{-\lambda x}\left[C_{19}(\sin \lambda x + \cos \lambda x) + C_{20}(\sin \lambda x - \cos \lambda x)\right] \\[4pt]
y_1'' = 2\lambda^2 e^{\lambda x}(-C_1 \sin \lambda x + C_2 \cos \lambda x) + 2\lambda^2 e^{-\lambda x}(C_3 \sin \lambda x - C_4 \cos \lambda x) \\
y_2'' = 2k\lambda^2 \left[e^{\lambda x}(-A_1 \sin \lambda x + A_2 \cos \lambda x) + e^{-\lambda x}(A_3 \sin \lambda x - A_4 \cos \lambda x)\right] + \frac{A_5 \cdot kx^2}{2} + 6C_5 x + 2C_6 \\
y_3'' = 2\lambda^2 e^{\lambda x}(-C_9 \sin \lambda x + C_{10} \cos \lambda x) + 2\lambda^2 e^{-\lambda x}(C_{11} \sin \lambda x - C_{12} \cos \lambda x) \\
y_4'' = 2\lambda^2 e^{\lambda x}(-C_{13} \sin \lambda x + C_{14} \cos \lambda x) + 2\lambda^2 e^{-\lambda x}(C_{15} \sin \lambda x - C_{16} \cos \lambda x) \\
y_5'' = 2\lambda^2 e^{\lambda x}(-C_{17} \sin \lambda x + C_{18} \cos \lambda x) + 2\lambda^2 e^{-\lambda x}(C_{19} \sin \lambda x - C_{20} \cos \lambda x) \\[4pt]
y_1''' = 2\lambda^3 e^{\lambda x}\left[-C_1(\cos \lambda x + \sin \lambda x) + C_2(\cos \lambda x - \sin \lambda x)\right] + 2\lambda^3 e^{-\lambda x}\left[C_3(\cos \lambda x - \sin \lambda x) + C_4(\sin \lambda x + \cos \lambda x)\right] \\
y_2''' = 2k\lambda^3 e^{\lambda x}\left[-A_1(\cos \lambda x + \sin \lambda x) + A_2(\cos \lambda x - \sin \lambda x)\right] + 2k\lambda^3 e^{-\lambda x}\left[A_3(\cos \lambda x - \sin \lambda x) + A_4(\sin \lambda x + \cos \lambda x)\right] \\
\quad + A_5 \cdot kx + 6C_5 \\
y_3''' = 2\lambda^3 e^{\lambda x}\left[-C_9(\cos \lambda x + \sin \lambda x) + C_{10}(\cos \lambda x - \sin \lambda x)\right] + 2\lambda^3 e^{-\lambda x}\left[C_{11}(\cos \lambda x - \sin \lambda x) + C_{12}(\sin \lambda x + \cos \lambda x)\right] \\
y_4''' = 2\lambda^3 e^{\lambda x}\left[-C_{13}(\cos \lambda x + \sin \lambda x) + C_{14}(\cos \lambda x - \sin \lambda x)\right] + 2\lambda^3 e^{-\lambda x}\left[C_{15}(\cos \lambda x - \sin \lambda x) + C_{16}(\sin \lambda x + \cos \lambda x)\right] \\
y_5''' = 2\lambda^3 e^{\lambda x}\left[-C_{17}(\cos \lambda x + \sin \lambda x) + C_{18}(\cos \lambda x - \sin \lambda x)\right] + 2\lambda^3 e^{-\lambda x}\left[C_{19}(\cos \lambda x - \sin \lambda x) + C_{20}(\sin \lambda x + \cos \lambda x)\right]
\end{cases}
\tag{17}
$$

Because of the continuity of the beam, the boundary conditions of the general solution for the deflection equation can be obtained as

$$
\begin{aligned}
&A: \begin{cases} y_1''(x=0) = 0 \\ y_1'''(x=0) = 0 \end{cases} \\[4pt]
&B: \begin{cases} y_1(x=l) = y_2(x=l) \\ y_1'(x=l) = y_2'(x=l) \\ y_1''(x=l) = y_2''(x=l) \\ y_1'''(x=l) = y_2'''(x=l) \end{cases} \\[4pt]
&C: \begin{cases} y_2(x=2l) = y_3(x=2l) \\ y_2'(x=2l) = y_3'(x=2l) \\ y_2''(x=2l) = y_3''(x=2l) \\ y_2'''(x=2l) = y_3'''(x=2l) \end{cases} \\[4pt]
&D: \begin{cases} y_3(x=3l) = y_4(x=3l) \\ y_3'(x=3l) = y_4'(x=3l) \\ y_3''(x=3l) = y_4''(x=3l) \\ y_3'''(x=3l) = y_4'''(x=3l) \end{cases} \\[4pt]
&E: \begin{cases} y_4(x=4l) = y_5(x=4l) \\ y_4'(x=4l) = y_5'(x=4l) \\ y_4''(x=4l) = y_5''(x=4l) \\ y_4'''(x=4l) = y_5'''(x=4l) \end{cases} \\[4pt]
&F: \begin{cases} y_5''(x=5l) = 0 \\ y_5'''(x=5l) = 0 \end{cases}
\end{aligned}
\tag{18}
$$

Eq. (18) is substituted into Eq. (17) in order to obtain the coefficient equations as follows

$$
\begin{aligned}
A&: \begin{cases} 2\lambda^3 e^{\lambda x}C_2 - 2\lambda^3 e^{-\lambda x}C_4 = 0 \\ 2\lambda^3 e^{\lambda x}(-C_1 + C_2) + 2\lambda^3 e^{-\lambda x}(C_3 + C_4) = 0 \end{cases} \\[6pt]
B&: \begin{cases}
e^{\lambda l}(C_1 \cos \lambda l + C_2 \sin \lambda l) + e^{-\lambda l}(C_3 \cos \lambda l + C_4 \sin \lambda l) \\
\quad = e^{\lambda l}(A_1 \cos \lambda l + A_2 \sin \lambda l) + e^{-\lambda l}(A_3 \cos \lambda l + A_4 \sin \lambda l)\cdot k + \frac{A_5 \cdot kl^4}{24} + C_5 l^3 + C_6 l^2 + C_7 l + C_8 \\
\lambda e^{\lambda l}\left[C_1(\cos \lambda l - \sin \lambda l) + C_2(\sin \lambda l + \cos \lambda l)\right] - \lambda e^{-\lambda l}\left[C_3(\sin \lambda l + \cos \lambda l) + C_4(\sin \lambda l - \cos \lambda l)\right] \\
\quad = k\lambda e^{\lambda l}\left[A_1(\cos \lambda l - \sin \lambda l) + A_2(\sin \lambda l + \cos \lambda l)\right] - \lambda e^{-\lambda l}\left[A_3(\sin \lambda l + \cos \lambda l) + A_4(\sin \lambda l - \cos \lambda l)\right] \\
\quad + \frac{A_5 \cdot kl^3}{6} + 3C_5 l^2 + 2C_6 l + C_7 \\
2k\lambda^2\left[e^{\lambda l}(-A_1 \sin \lambda l + A_2 \cos \lambda l) + e^{-\lambda l}(A_3 \sin \lambda l - A_4 \cos \lambda l)\right] + \frac{A_5 \cdot kl^2}{2} + 6C_5 l + 2C_6 \\
\quad = 2\lambda^2 e^{\lambda l}(-C_9 \sin \lambda l + C_{10} \cos \lambda l) + 2\lambda^2 e^{-\lambda l}(C_{11} \sin \lambda l - C_{12} \cos \lambda l) \\
2\lambda^3 e^{\lambda l}\left[-C_1(\cos \lambda l + \sin \lambda l) + C_2(\cos \lambda l - \sin \lambda l)\right] + 2\lambda^3 e^{-\lambda l}\left[C_3(\cos \lambda l - \sin \lambda l) + C_4(\sin \lambda l + \cos \lambda l)\right] \\
\quad = 2k\lambda^3 e^{\lambda l}\left[-A_1(\cos \lambda l + \sin \lambda l) + A_2(\cos \lambda l - \sin \lambda l)\right] \\
\quad + 2k\lambda^3 e^{-\lambda l}\left[A_3(\cos \lambda l - \sin \lambda l) + A_4(\sin \lambda l + \cos \lambda l)\right] + A_5 \cdot kl + 6C_5
\end{cases}
\end{aligned}
\tag{19}
$$

$$C: \begin{cases} e^{2\lambda l}(A_5\cos 2\lambda l + A_6\sin 2\lambda l) + e^{-2\lambda l}(A_7\cos 2\lambda l + A_8\sin 2\lambda l)\cdot k + \dfrac{2A_1\cdot kl^4}{3} + 8C_3 l^3 + 4C_4 l^2 + 2C_5 l + C_6 \\[4pt]
= e^{2\lambda l}(C_9\cos 2\lambda l + C_{10}\sin 2\lambda l) + e^{-2\lambda l}(C_{11}\cos 2\lambda l + C_{12}\sin 2\lambda l) \\[4pt]
k\lambda e^{2\lambda l}\left[A_5(\cos 2\lambda l - \sin 2\lambda l) + A_6(\sin 2\lambda l + \cos 2\lambda l)\right] - \lambda e^{-2\lambda l}\left[A_7(\sin 2\lambda l + \cos 2\lambda l) + A_8(\sin 2\lambda l - \cos 2\lambda l)\right] \\[2pt]
\quad + \dfrac{4A_1\cdot kl^3}{3} + 12C_3 l^2 + 4C_4 l + C_7 \\[4pt]
= \lambda e^{2\lambda l}\left[C_9(\cos 2\lambda l - \sin 2\lambda l) + C_{10}(\sin 2\lambda l + \cos 2\lambda l)\right] - \lambda e^{-2\lambda l}\left[C_{11}(\sin 2\lambda l + \cos 2\lambda l) + C_{12}(\sin 2\lambda l - \cos 2\lambda l)\right] \\[4pt]
2k\lambda^2\left[e^{2\lambda l}(-A_5\sin 2\lambda l + A_6\cos 2\lambda l) + e^{-2\lambda l}(A_7\sin 2\lambda l - A_8\cos 2\lambda l)\right] + 2A_1\cdot kl^2 + 12C_3 l + 2C_4 \\[4pt]
= 2\lambda^2 e^{2\lambda l}(-C_9\sin 2\lambda l + C_{10}\cos 2\lambda l) + 2\lambda^2 e^{-2\lambda l}(C_{11}\sin 2\lambda l - C_{12}\cos 2\lambda l) \\[4pt]
2k\lambda^2 e^{2\lambda l}\left[-A_5(\cos 2\lambda l + \sin 2\lambda l) + A_6(\cos 2\lambda l - \sin 2\lambda l)\right] + 2k\lambda^3 e^{-2\lambda l}\left[A_7(\cos 2\lambda l - \sin 2\lambda l) + A_8(\sin 2\lambda l + \cos 2\lambda l)\right] \\[2pt]
\quad + 2A_1\cdot kl + 6C_3 \\[4pt]
= 2\lambda^3 e^{2\lambda l}\left[-C_9(\cos 2\lambda l + \sin 2\lambda l) + C_{10}(\cos 2\lambda l - \sin 2\lambda l)\right] + 2\lambda^3 e^{-2\lambda l}\left[C_{11}(\cos 2\lambda l - \sin 2\lambda l) + C_{12}(\sin 2\lambda l + \cos 2\lambda l)\right] \end{cases}$$

$$D: \begin{cases} e^{3\lambda l}(C_9\cos 3\lambda l + C_{10}\sin 3\lambda l) + e^{-3\lambda l}(C_{11}\cos 3\lambda l + C_{12}\sin 3\lambda l) \\[4pt]
= e^{3\lambda l}(C_{13}\cos 3\lambda l + C_{14}\sin 3\lambda l) + e^{-3\lambda l}(C_{15}\cos 3\lambda l + C_{16}\sin 3\lambda l) + \dfrac{q}{k} \\[4pt]
\lambda e^{3\lambda l}\left[C_9(\cos 3\lambda l - \sin 3\lambda l) + C_{10}(\sin 3\lambda l + \cos 3\lambda l)\right] - \lambda e^{-3\lambda l}\left[C_{11}(\sin 3\lambda l + \cos 3\lambda l) + C_{12}(\sin 3\lambda l - \cos 3\lambda l)\right] \\[4pt]
= \lambda e^{3\lambda l}\left[C_{13}(\cos 3\lambda l - \sin 3\lambda l) + C_{14}(\sin 3\lambda l + \cos 3\lambda l)\right] - \lambda e^{-3\lambda l}\left[C_{15}(\sin 3\lambda l + \cos 3\lambda l) + C_{16}(\sin 3\lambda l - \cos 3\lambda l)\right] \\[4pt]
2\lambda^2 e^{3\lambda l}(-C_9\sin 3\lambda l + C_{10}\cos 3\lambda l) + 2\lambda^2 e^{-3\lambda l}(C_{11}\sin 3\lambda l - C_{12}\cos 3\lambda l) \\[4pt]
= 2\lambda^2 e^{3\lambda l}(-C_{13}\sin 3\lambda l + C_{14}\cos 3\lambda l) + 2\lambda^2 e^{-3\lambda l}(C_{15}\sin 3\lambda l - C_{16}\cos 3\lambda l) \\[4pt]
2\lambda^3 e^{3\lambda l}\left[-C_9(\cos 3\lambda l + \sin 3\lambda l) + C_{10}(\cos 3\lambda l - \sin 3\lambda l)\right] + 2\lambda^3 e^{-3\lambda l}\left[C_{11}(\cos 3\lambda l - \sin 3\lambda l) + C_{12}(\sin 3\lambda l + \cos 3\lambda l)\right] \\[4pt]
= 2\lambda^3 e^{3\lambda l}\left[-C_{13}(\cos 3\lambda l + \sin 3\lambda l) + C_{14}(\cos 3\lambda l - \sin 3\lambda l)\right] + 2\lambda^3 e^{-3\lambda l}\left[C_{15}(\cos 3\lambda l - \sin 3\lambda l) + C_{16}(\sin 3\lambda l + \cos 3\lambda l)\right] \end{cases}$$

$$(19)$$

$$E: \begin{cases} e^{4\lambda l}(C_{13}\cos 4\lambda l + C_{14}\sin 4\lambda l) + e^{-4\lambda l}(C_{15}\cos 4\lambda l + C_{16}\sin 4\lambda l) + \dfrac{q}{k} \\[4pt]
= e^{4\lambda l}(C_{17}\cos 4\lambda l + C_{18}\sin 4\lambda l) + e^{-4\lambda l}(C_{19}\cos 4\lambda l + C_{20}\sin 4\lambda l) \\[4pt]
\lambda e^{4\lambda l}\left[C_{13}(\cos 4\lambda l - \sin 4\lambda l) + C_{14}(\sin 4\lambda l + \cos 4\lambda l)\right] - \lambda e^{-4\lambda l}\left[C_{15}(\sin 4\lambda l + \cos 4\lambda l) + C_{16}(\sin 4\lambda l - \cos 4\lambda l)\right] \\[4pt]
= \lambda e^{4\lambda l}\left[C_{17}(\cos 4\lambda l - \sin 4\lambda l) + C_{18}(\sin 4\lambda l + \cos 4\lambda l)\right] - \lambda e^{-4\lambda l}\left[C_{19}(\sin 4\lambda l + \cos 4\lambda l) + C_{20}(\sin 4\lambda l - \cos 4\lambda l)\right] \\[4pt]
2\lambda^2 e^{4\lambda l}(-C_{13}\sin 4\lambda l + C_{14}\cos 4\lambda l) + 2\lambda^2 e^{-4\lambda l}(C_{15}\sin 4\lambda l - C_{16}\cos 4\lambda l) \\[4pt]
= 2\lambda^2 e^{4\lambda l}(-C_{17}\sin 4\lambda l + C_{18}\cos 4\lambda l) + 2\lambda^2 e^{-4\lambda l}(C_{19}\sin 4\lambda l - C_{20}\cos 4\lambda l) \\[4pt]
2\lambda^3 e^{4\lambda l}\left[-C_{13}(\cos 4\lambda l + \sin 4\lambda l) + C_{14}(\cos 4\lambda l - \sin 4\lambda l)\right] + 2\lambda^3 e^{-4\lambda l}\left[C_{15}(\cos 4\lambda l - \sin 4\lambda l) + C_{16}(\sin 4\lambda l + \cos 4\lambda l)\right] \\[4pt]
= 2\lambda^3 e^{4\lambda l}\left[-C_{17}(\cos 4\lambda l + \sin 4\lambda l) + C_{18}(\cos 4\lambda l - \sin 4\lambda l)\right] + 2\lambda^3 e^{-4\lambda l}\left[C_{19}(\cos 4\lambda l - \sin 4\lambda l) + C_{20}(\sin 4\lambda l + \cos 4\lambda l)\right] \end{cases}$$

$$F: \begin{cases} 2\lambda^2 e^{5\lambda l}(-C_{17}\sin 5\lambda l + C_{18}\cos 5\lambda l) + 2\lambda^2 e^{-5\lambda l}(C_{19}\sin 5\lambda l - C_{20}\cos 5\lambda l) = 0 \\[4pt]
2\lambda^3 e^{5\lambda l}\left[-C_{17}(\cos 5\lambda l + \sin 5\lambda l) + C_{18}(\cos 5\lambda l - \sin 5\lambda l)\right] + 2\lambda^3 e^{-5\lambda l}\left[C_{19}(\cos 5\lambda l - \sin 5\lambda l) + C_{20}(\sin 5\lambda l + \cos 5\lambda l)\right] = 0 \end{cases}$$